Title: A molecular and spatial resource defining tubulin isotype organization during corneal development

Authors: Ramarapu R*[1,2], Stoehr WR*[1,2], Miesen M[1,2], Border, S.[2], Thomasy SM[±1,3], and Rogers CD[±2]

* These authors contributed to this manuscript equally
[±]Corresponding authors
smthomasy@ucdavis.edu
crdrogers@ucdavis.edu

Affiliations:
[1]Department of Surgical and Radiological Sciences, School of Veterinary Medicine, University of California, 1 Shields Ave., Davis, CA, 95616, USA.
[2] Department of Anatomy, Physiology, and Cell Biology, School of Veterinary Medicine, University of California, Davis, Davis, CA, 95616, USA
[3] Department of Ophthalmology and Vision Science, School of Medicine, University of California Davis, Davis, CA, 95616, USA.

Keywords: neural crest, cornea, tubulin, microtubules, endothelium, stroma

ABSTRACT

Microtubules are essential components of the cytoskeleton that support epithelial organization, polarity, and tissue morphogenesis. They are composed of α- and β-tubulin heterodimers, each encoded by distinct genes that generate closely related but functionally distinct isotypes. Although several tubulin isotypes have been implicated in ocular development and disease, how isotype diversity is organized during corneal morphogenesis remains poorly defined. Herein, we use the developing chick embryo as a model system to investigate the conservation and spatiotemporal localization of tubulin isotypes during corneal development. Through comparative amino acid sequence analysis, we show that chick and human α- and β-tubulin isotypes are highly conserved at structural and catalytic domains, with divergence concentrated in C-terminal regions associated with post-translational modifications. To relate these molecular features to tissue-level organization, we performed a longitudinal immunohistochemical analysis of five tubulin isotypes across key stages of corneal development. We identify distinct and dynamic patterns of isotype enrichment along apico-basal and central-peripheral axes within the cornea, as well as isotype-specific redistribution during epithelial maturation and corneal endothelial differentiation. Notably, TUBA5/TUBA4A exhibits tightly regulated localization, including enrichment at the leading edge of migratory corneal stromal progenitor cells and within the maturing corneal endothelium. Together, these data establish the chick embryo as a conserved and tractable model for studying tubulin isotype diversity in the cornea, and more broadly across other tissues, and to provide a developmental resource linking tubulin sequence identity to spatially defined microtubule organization during epithelial morphogenesis.

SUMMARY STATEMENT

This study defines when and where distinct tubulin proteins are deployed during corneal development, providing a resource for understanding cytoskeletal organization in the developing eye.

INTRODUCTION

The cornea is the transparent anterior tissue of the eye and plays a central role in light refraction, optical clarity, and protection of the ocular surface. Its development requires the coordinated morphogenesis of three distinct layers, the stratified epithelium, the collagen-rich stroma, and the corneal endothelial monolayer, each of which emerges through tightly regulated processes of cell migration, polarization, differentiation, and tissue-scale organization (Kivela and Uusitalo 1998, Eghrari, Riazuddin et al. 2015, Chen and Dong 2022). Underlying these events is a dynamic cytoskeletal network that integrates mechanical support with intracellular transport and signaling (Weinreb and Ryder 1990, Su, Desikan et al. 2025).

Microtubules are a core component of this cytoskeletal network and are essential for epithelial organization, directional migration, vesicle trafficking, and force generation (Laan, Husson et al. 2008, Garcin and Straube 2019). They are assembled from heterodimers of α- and β-tubulin, two highly conserved protein families encoded by multiple genes that give rise to distinct isotypes. Although tubulin isotypes differ by only a small number of amino acids, accumulating evidence indicates that these differences, together with extensive post-translational modifications (PTMs), generate functionally specialized microtubule populations across tissues and developmental contexts (Hausrat, Radwitz et al. 2021, Moutin, Bosc et al. 2021, Bar, Popp et al. 2022, Carmona, Marinho et al. 2023). This concept, often referred to as the “tubulin code,” proposes that isotype composition and PTMs tune microtubule stability, interactions with motors and microtubule-associated proteins (MAPs), and intracellular organization.

Spatiotemporal expression of tubulin isotypes has been most extensively characterized in the nervous system, where mutations in both α- and β-tubulin genes cause a spectrum of developmental disorders collectively termed tubulinopathies. These conditions routinely affect the central nervous system and include cortical malformations, axon guidance defects, epilepsy, hypomyelination, and corpus callosum abnormalities (Aiken, Buscaglia et al. 2017, Schroter, Doring et al. 2021, Schroter, Popp et al. 2022, Ganne, Balasubramaniam et al. 2023, Torella, Ricca et al. 2023, Benkirane, Bonhomme et al. 2024, Wan, Zhou et al. 2024). By contrast, the roles of tubulin isotypes in ocular development, specifically in the cornea, remain limited. Emerging clinical and experimental evidence suggests that this gap in knowledge is noteworthy (Table 1). Mutations in *TUBB3* underlie congenital fibrosis of the extraocular muscles, a disorder characterized by impaired ocular motility and structural abnormalities (Chew, Balasubramanian et al. 2013, Whitman, Andrews et al. 2016). *De novo* mutations in *TUBA3D* have been associated with keratoconus (Hao, Chen et al. 2017), which affects cornea shape and function. Additionally, recent work has linked microtubule dysregulation, including altered *TUBB4A* expression, to Fuchs’ endothelial corneal dystrophy downstream of TCF4 activity (Yan, Mehta et al. 2024). Together, these findings point to previously underappreciated roles for tubulin isotypes in corneal morphogenesis and homeostasis.

The chick embryo provides a powerful system to address the role of tubulin function during development. Chick corneal development is highly accessible, follows a well-defined temporal sequence, and is morphogenetically conserved with human ocular development (Ritchey, Code et al. 2011, Lwigale 2015). Moreover, the chick has long served as a model for studying periocular mesenchyme migration, epithelial-mesenchymal interactions, and corneal layer specification. However, a systematic resource describing tubulin isotype conservation and spatiotemporal localization during corneal development is currently lacking.

Here, we present a combined computational and experimental resource characterizing the spatiotemporal localization of several α- and β-tubulin isotypes in the developing chick cornea. We first perform a comparative sequence analysis of chick and human tubulin isotypes to assess conservation, phylogenetic relationships, and predicted PTM availability. We then provide a longitudinal spatiotemporal map of five tubulin isotypes (TUBA1A, TUBA1B, TUBA5/TUBA4A, TUBB1/TUBB2A, and TUBB4/TUBB3) using immunohistochemistry (IHC) across key stages of corneal development. Together, these data establish the chick as a robust model for studying isotype-specific microtubule biology in the cornea as well as other epithelial and mesenchymal tissues and provide a foundational framework for future functional and disease-oriented studies.

Table 1. Congenital Ocular Tubulinopathies

Gene	Disease/Context	Methodology	Reference
TUBA1A	Elevated in vitreous humor (± pathologic myopia)	Proteomics; ELISA	(Wen, Ren et al. 2024)
	De novo mutation associated with congenital cataract	WGS (case study)	(Myers, Bello-Espinosa et al. 2015)
	Enriched in Descemet's membrane in FECD	Shotgun proteomics	(Nakagawa, Okumura et al. 2023)
TUBA1B	Downregulated in metastatic uveal melanoma	Two-dimensional difference gel electrophoresis, IHC, western blot (WB)	(Linge, Kennedy et al. 2012)
TUBA3D	Mutation associated with keratoconus	Whole exome sequencing (WES), WB, qPCR, IF and flow cytometry	(Hao, Chen et al. 2017)
TUBA4	Increased acetylated TUBA4A in glaucomatous TM	IHC, WB	(Su, Desikan et al. 2025)
TUBB/TUBB5	Increased TUBB abundance in keratoconus cornea	LC-MS/MS (proteomics)	(Joseph, Srivastava et al. 2011)
TUBB3	Mutation associated with congenital cataract	WES (case study)	(Yeniay Sut, Yildirim et al. 2022)
	A302T mutation causes congenital fibrosis of extraocular muscles	Case studies with genome sequencing	(Tischfield, Baris et al. 2010)
TUBB4B	Upregulated in FECD	Bulk RNA-seq; WB; IHC	(Yan, Mehta et al. 2024)

RESULTS

Conservation of tubulin isotype sequences between chick and human

To evaluate the extent to which chick tubulin isotypes model their human counterparts, and to identify sequence features that may underlie isotype-specific function, we aligned all RefSeq α- and β-tubulin protein sequences from *Homo sapiens* (human) and *Gallus gallus* (chicken) (Table 2). Analyses were performed separately for α- and β-tubulins and included multiple sequence alignment, per-residue heterogeneity scoring, phylogenetic reconstruction, and pairwise identity comparisons.

Multiple sequence alignments revealed a high degree of conservation across both species for all tubulin isotypes, with a majority of sequence divergence confined to the N- and/or C-terminal tails depending on subtype (Fig. 1A,B; Fig. 2A,B). By contrast, the globular core domains, including residues involved in GTP binding and heterodimer formation, were nearly identical. Quantification of per-residue heterogeneity confirmed this pattern, with minimal divergence across the folded core and sharply increased variability toward the C-termini of both α- and β-tubulins (Fig. 1A,B; Fig. 2A,B).

Phylogenetic analysis further demonstrated that tubulin sequences clustered primarily by isotype rather than by species, indicating strong evolutionary constraint on isotype identity (Fig. 1C; Fig. 2C). With the exception of the closely related TUBB2A/B pair, chick and human orthologs consistently formed tight cross-species clades. Pairwise identity matrices reinforced these relationships, with orthologous chick-human pairs exhibiting the highest amino acid identity, often exceeding 98% (Fig. 1C,D; Fig. 2C,D).

Mapping of canonical and predicted PTM sites onto the aligned sequences revealed broad conservation of putative modification sites within the globular domains, including residues associated with acetylation, methylation, and phosphorylation (Fig. 1E; Fig. 2E). By contrast, residues governing C-terminal detyrosination, polyglutamylation, and polyglycylation varied substantially among isotypes. Notably, the canonical Tyr-Glu-Glu motif required for α-tubulin tyrosination/detyrosination cycling was altered or absent in TUBA5/TUBA4A and the TUBAL3/TUBA8 group, suggesting isotype-specific constraints on tail-based PTM dynamics (Fig. 1E). Detailed alignment of C-terminal tails further revealed isotype-specific differences in tail length and charge distribution, with α-tubulins showing greater variability than β-tubulins (Fig. 1F; Fig. 2F).

Together, these analyses demonstrate that chick and human tubulin isotypes are highly conserved at structural and catalytic sites while diverging in their C-terminal tails, supporting the use of the chick as a model for investigating isotype-specific microtubule function and providing a molecular framework for interpreting tissue-level localization patterns.

Table 2. Tubulin Nomenclature

Human Protein	Human NCBI Reference Sequence	Chick Protein Homolog	Chick NCBI Reference Sequence	Percent Identical
TUBA1A	NP_001257328.1	TUBA1A	NP_001292201.2	100%
TUBA1B	NP_006073.2	TUBA1B	XP_015155803.1	100%
TUBA4A	NP_005991.1	TUBA5	NP_001383566.1	97.54%
TUBB2A	NP_001060.1	TUBB1	XP_040520935.1	99.33%
TUBB3	NP_006077.2	TUBB4	NP_001383082.1	99.78%

Spatiotemporal localization of TUBA1A during corneal development

To define the spatial and temporal distribution of TUBA1A during corneal development, we performed IHC on chick embryos from embryonic day (E)3 through E14, encompassing corneal epithelial specification, periocular mesenchyme migration, stromal formation, and tissue maturation. At E3, TUBA1A immunoreactivity was detected in the apical region of the surface ectoderm, corresponding to the presumptive corneal epithelium, as well as in the lens epithelium (Fig. 3A-D). This pattern persisted through E4 and E5, during which periocular mesenchyme migration gives rise to the presumptive corneal endothelium and stroma (Fig. 3E-L). By E6, when distinct corneal layers are established, TUBA1A was present throughout the epithelium, stroma, and endothelium, with comparatively stronger signal in the corneal endothelium (Fig. 3M-P).

In the maturing E14 cornea, TUBA1A exhibited robust expression in the stratifying corneal epithelium and stromal keratocytes (Fig. 3Q-X). Within the corneal endothelium, TUBA1A signal was enriched centrally and diminished toward the periphery, indicating a spatial gradient across the tissue (Fig. 3U-X). These data demonstrate that TUBA1A is broadly expressed throughout corneal development but exhibits dynamic changes in subcellular localization and tissue distribution over time.

Spatiotemporal localization of TUBA1B during corneal development

To compare the spatial distribution of closely related α-tubulin isotypes, we next examined the expression of TUBA1B across corneal development. The IHC analysis revealed that, although TUBA1B is broadly expressed, its localization pattern differs from that of TUBA1A. At E3, TUBA1B immunoreactivity was detected at low levels throughout the surface ectoderm and lens epithelium, with a distinct band of enrichment along the apical surface of the presumptive corneal epithelium (Fig. 4A-D). This apical bias persisted at E4 and E5, during which TUBA1B remained broadly distributed across the developing corneal epithelium while also appearing in the presumptive corneal endothelium following periocular mesenchyme migration (Fig. 4E-L).

By E6, when corneal layers are clearly established, TUBA1B exhibited a broadly cytoplasmic distribution throughout the corneal epithelium, stroma, and endothelium (Fig. 4M-P). In the mature E14 cornea, TUBA1B remained robustly expressed in the stratifying corneal epithelium and stromal keratocytes (Fig. 4Q-X). In contrast to TUBA1A, TUBA1B displayed relatively uniform expression across the corneal endothelium, with no pronounced central-peripheral gradient (Fig. 4U-X). These observations indicate that TUBA1B is a broadly expressed α-tubulin isotype throughout corneal development, with consistent enrichment in the epithelium and comparatively uniform distribution within the endothelium.

Spatiotemporal localization of TUBA5 (ortholog to human TUBA4A) during corneal development

To further compare α-tubulin isotype distribution during corneal morphogenesis, we examined the expression of TUBA5/TUBA4A across developmental stages. IHC analysis revealed that TUBA5/TUBA4A exhibits dynamic and spatially restricted localization patterns during corneal development. At E3, prior to periocular mesenchyme migration, TUBA5/TUBA4A expression was confined to the surface ectoderm, with strong enrichment at the apical surface of the presumptive corneal epithelium (Fig. 5A-D). This apical localization was maintained at E4, with increased overall signal intensity in the epithelium (Fig. 5E-H). By E5, following the first wave of periocular mesenchyme migration, TUBA5/TUBA4A was detected in both the corneal epithelium and the presumptive corneal endothelium (Fig. 5I-P). Elevated signal was also observed in the anterior periocular mesenchyme contiguous with the forming endothelial layer (Fig. 5I-P, arrow).

At E6, when corneal layers are established, TUBA5/TUBA4A localization shifted toward a more basal distribution within both the corneal epithelium and endothelium (Fig. 5O-AB). Expression remained evident in the anterior periocular mesenchyme corresponding to the second wave of migratory stromal precursors (Fig. 5Y-AB). In the mature E14 cornea, TUBA5/TUBA4A expression was largely restricted to the corneal epithelium and endothelium, with minimal stromal signal (Fig. 5AC-AJ). Within the corneal endothelium, TUBA5/TUBA4A displayed higher expression centrally relative to the periphery and exhibited an apical bias within endothelial cells (Fig. 5AG-AJ). These observations indicate that TUBA5/TUBA4A undergoes marked redistribution during corneal development and exhibits region-specific patterning within the corneal endothelium.

To further resolve TUBA5/TUBA4A localization at cellular resolution, we performed corneal flat-mount imaging at E6, focusing on the corneal endothelium and migratory periocular mesenchyme. Confocal Z-stack maximum intensity projections revealed a diffuse peri-membranous pattern of TUBA5/TUBA4A staining across the epithelialized endothelial monolayer when visualized together with the junctional marker N-cadherin (NCAD) (Fig. 6A- D'). In dividing endothelial cells, TUBA5/TUBA4A signal was enriched in microtubule structures associated with separating chromatin (Fig. 6B, B', D, D'). In the migratory periocular mesenchyme, TUBA5/TUBA4A labeled prominent microtubule bundles of variable diameter (Fig. 6E-H'), which were particularly evident at the leading edge of the migratory population (Fig. 6F, F'). The NCAD staining in these cells appeared more diffuse and included cytosolic puncta (Fig. 6E'-H'). Together, these data demonstrate that TUBA5/TUBA4A exhibits dynamic subcellular localization patterns in both epithelialized endothelial cells and migratory mesenchymal populations during corneal development.

Spatiotemporal localization of TUBB1 (ortholog to human TUBB2A) during corneal development

To assess β-tubulin isotype distribution during corneal morphogenesis, we examined the localization of TUBB2A across developmental stages. TUBB1/TUBB2A exhibited broad expression but with notable temporal changes in epithelial localization. At E3, TUBB1/TUBB2A immunoreactivity was detected throughout the surface ectoderm and lens epithelium, with modest enrichment at the apical surface of the presumptive corneal epithelium (Fig. 7A-D). This pattern was maintained at E4, with continued expression in the epithelium and migrating periocular mesenchyme (Fig. 7E-H). By E5, following establishment of the presumptive corneal endothelium, TUBB1/TUBB2A expression decreased at the apical epithelial surface and became more prominent within endothelial cells (Fig. 7I-L).

At E6, TUBB1/TUBB2A remained broadly expressed across the corneal epithelium, stroma, and endothelium, with a predominantly cytoplasmic distribution and reduced epithelial apical bias (Fig. 7M-P). In the mature E14 cornea, TUBB1/TUBB2A expression increased at the apical surface of the stratified corneal epithelium and remained robust within stromal keratocytes (Fig. 7Q-X). Within the corneal endothelium, TUBB1/TUBB2A was expressed throughout the tissue, with higher signal intensity centrally relative to the periphery and an apical bias in central endothelial cells (Fig. 7U-X). These findings indicate that TUBB1/TUBB2A undergoes developmental redistribution within the corneal epithelium while maintaining broad expression in the corneal endothelium, with emerging spatial gradients during tissue maturation.

.

Spatiotemporal localization of TUBB4 (ortholog to human TUBB3) during corneal development

Finally, we examined the expression of TUBB4/TUBB3, a neuron-associated β-tubulin isotype, to determine its distribution within corneal tissues. TUBB4/TUBB3 displayed a highly polarized and developmentally persistent localization pattern. At E3, TUBB4/TUBB3 immunoreactivity was detected in the surface ectoderm,

corresponding to the presumptive corneal epithelium (Fig. 8A-D). The TUBB4/TUBB3 signal then became apically distributed at E4 and E5, with low to moderate expression observed in the migrating periocular mesenchyme and developing corneal endothelium at E5 (Fig. 8E-L). At E6, TUBB4/TUBB3 continued to exhibit strong apical epithelial localization, while endothelial expression remained low (Fig. 8M-P).

In the mature E14 cornea, TUBB4/TUBB3 was strongly enriched at the apical surface of the stratified corneal epithelium and within the corneal endothelium (Fig. 8Q-T). In addition, prominent TUBB4/TUBB3-positive tracks were observed within the anterior stroma, consistent with developing corneal nerves. Analysis of endothelial localization revealed a central-peripheral gradient, with higher TUBB4/TUBB3 expression centrally and an apical bias within endothelial cells (Fig. 8U-X). These results demonstrate that TUBB4/TUBB3 marks apical microtubule populations in the corneal epithelium throughout development and becomes increasingly associated with central endothelial regions and stromal innervation during corneal maturation.

Discussion

In this study, we present a cross-species and developmental resource quantifying tubulin isotype conservation together with spatiotemporal localization during corneal morphogenesis in the chick embryo. Through comparative sequence analysis, we demonstrate that chick and human α- and β-tubulin isotypes are highly conserved at structural and catalytic domains, while diverging in their N- and/or C-terminal tails. Using longitudinal IHC in chick embryos, we show that individual isotypes exhibit distinct and dynamic localization patterns across corneal tissues. Together, these data establish the chick embryo as a robust model for investigating isotype-specific microtubule biology using the cornea as a tissue exemplar and provide a framework for future functional and disease-oriented studies.

Our comparative sequence analyses revealed that both α- and β-tubulin families cluster by isotype rather than by species, underscoring strong evolutionary constraint on isotype identity (Fig. 1, 2). The near-complete conservation of GTP-binding cores and heterodimerization interfaces suggests that potential isotype-specific behavior is unlikely to arise from differences in catalytic activity (Downing and Nogales 1998, Kristensson 2021, Kalutskii, Grubmuller et al. 2025). Instead, sequence divergence is concentrated within the N- and/or C-terminal tails, consistent with nucleotide binding domains (Yon, Ha et al. 2025) and the established role of C-termini as platforms for PTMs and interactions with motor proteins and MAPs (Gadadhar, Bodakuntla et al. 2017, Janke and Magiera 2020, Bao, Dorig et al. 2023). Mapping of canonical and predicted PTM sites further supports this view, as modification sites within the globular core are largely conserved, whereas residues governing detyrosination, polyglutamylation, and polyglycylation vary across isotypes. These features align with the “tubulin code” paradigm, in which isotype composition and PTM patterns generate functionally distinct microtubule populations without altering the underlying polymerization machinery (Verhey and Gaertig 2007, Janke 2014, Wethekam and Moore 2022, Magiera 2023).

Two observations warrant emphasis in the context of corneal development. First, α-tail detyrosination logic varies among isotypes. Isotypes with intact Tyr-Glu-Glu termini can cycle through tyrosination/Δ2/Δ3 states that stabilize microtubules and modulate motor traffic (Bar, Popp et al. 2022, Sanyal, Pietsch et al. 2023). Isotypes such as TUBA4A and the TUBAL3/TUBA8 group may restrict this cycle, creating layer-specific pools of stable microtubules. This postulate is consistent with the robust TUBA5/TUBA4A staining seen in the corneal epithelium and endothelium. Second, β-isotypes showed fewer active site deviations but retain tail diversity that could shape polyglutamylation/polyglycylation, tuning axoneme-like or epithelial arrays during corneal morphogenesis (Yang et al. 2021). These observations correspond with the growing recognition that microtubule PTMs regulate trafficking, force generation, and epithelial architecture during development and disease (Liu, Chen et al. 2022, Carmona, Marinho et al. 2023). They also align with reports linking microtubule

dysregulation to human corneal pathology, such as Fuchs' endothelial corneal dystrophy, motivating the study of targeted structural and functional analysis in the corneal endothelium (Yan, Mehta et al. 2024).

Within this molecular framework, our IHC analyses reveal that tubulin isotypes are not uniformly distributed during corneal development but instead exhibit distinct spatial, temporal, and subcellular localization patterns. Apical microtubule networks are a conserved scaffold beneath the apical membrane that integrate with actin and intermediate filament systems to support planar cell polarity, ciliogenesis and directional trafficking (Fernandes, McCormack et al. 2014, Takeda, Sami et al. 2018, Plochocka, Ramirez Moreno et al. 2021). Among α-tubulins, TUBA1A and TUBA1B are broadly expressed across corneal layers, consistent with roles in maintaining core microtubule architecture during epithelial morphogenesis. However, these closely related isotypes differ in their spatial organization: TUBA1A displays dynamic changes in epithelial localization and central-peripheral gradients within the corneal endothelium, whereas TUBA1B shows more uniform endothelial distribution and persistent apical enrichment in epithelial cells (Fig. 3, 4).These observations support the idea that even highly conserved α-isotypes contribute to distinct microtubule populations within the same tissue.

TUBA5/TUBA4A exhibits the most dynamic and spatially restricted pattern among the α-tubulins examined (Fig. 5). Its early apical enrichment in the presumptive corneal epithelium, transient expression in migrating periocular mesenchyme, and later restriction to epithelial and endothelial compartments, coupled with pronounced central-peripheral gradients in the endothelium, point to tightly regulated deployment during morphogenesis. Notably, TUBA5/TUBA4A lacks the canonical C-terminal tyrosination motif present in most α-tubulins, suggesting that its incorporation may generate microtubule populations with altered PTM cycling and stability (Paturle-Lafanechere, Manier et al. 1994, Janke and Magiera 2020). Differences in TUBA5/TUBA4A microtubule morphology were identified between epithelialized corneal endothelia and the migratory mesenchyme suggestive of overlapping structural roles in both cell states. The localization of TUBA5/TUBA4A at the leading edge of migratory corneal progenitors and within the maturing endothelium is consistent with roles in stabilizing microtubule arrays during collective cell migration and in maintaining long-lived epithelial monolayers (Etienne-Manneville 2013, Bar, Popp et al. 2022).

In contrast to α-tubulins, β-tubulin isotypes displayed sharper spatial biases. TUBB1/TUBB2A is broadly expressed across corneal tissues but undergoes developmental redistribution within the epithelium, transitioning from early apical enrichment to a more cytoplasmic pattern and later re-establishing apical localization during epithelial stratification (Fig. 6). Within the corneal endothelium, TUBB1/TUBB2A remains robustly expressed and develops a central-peripheral gradient during maturation. TUBB4/TUBB3, although classically associated with neuronal microtubules (Katsetos, Herman et al. 2003, Jouhilahti, Peltonen et al. 2008), has also previously been identified in non-neuronal migratory neural crest cell populations (Chacon and Rogers 2019). TUBB4/TUBB3 shows persistent apical enrichment in the corneal epithelium throughout development and becomes increasingly prominent in central endothelial regions and stromal nerve tracks at later stages. These patterns suggest that β-isotypes may preferentially mark dynamic, polarized, or transport-competent microtubule populations within the cornea.

Some organizational themes emerge from integrating these findings. First, apical enrichment of multiple tubulin isotypes, including TUBA1B and TUBB4/TUBB3, highlights the importance of specialized subapical microtubule arrays in corneal epithelial polarity. Second, the emergence of central-peripheral gradients within the corneal endothelium, particularly for α-isotypes such as TUBA1A and TUBA5/TUBA4A, suggests regional tuning of microtubule stability within this mechanically and metabolically demanding tissue. The corneal endothelium relies on long-lived microtubules to sustain vesicle trafficking and junctional integrity, and differential isotype composition may contribute to these regional functional demands (Bonanno 2012).

Importantly, the developmental patterns described here intersect with emerging links between microtubule dysregulation and human corneal disease. Altered tubulin expression and microtubule remodeling have been implicated in the pathogenesis of Fuchs' endothelial corneal dystrophy and other corneal disorders, and mutations in multiple tubulin genes are now associated with ocular phenotypes (Tischfield, Cederquist et al. 2011, Ong Tone, Kocaba et al. 2021). The conservation of tubulin isotypes and their developmental deployment in the chick cornea underscores the utility of this model for probing how isotype composition and PTM states contribute to corneal homeostasis and disease susceptibility.

In summary, this work provides a foundational resource integrating tubulin isotype sequence conservation with tissue-level localization during corneal development. By establishing conserved molecular features and defining when and where specific tubulin isotypes are deployed, we lay the groundwork for future mechanistic studies investigating how microtubule diversity shapes epithelial morphogenesis and how its disruption contributes to pathology in the cornea and other tissues.

MATERIALS AND METHODS

Sequence Analysis

All FASTA protein sequences were collected from the NCBI RefSeq database and aligned within the alpha- and beta-tubulin subtypes using the *msa* package in R. All subsequent computations were performed in R using these aligned sequences. Dendrograms were created using a neighbor-joining tree estimation algorithm using the *ape* package and further visualized using the *ggtree* package. Multiple sequence alignments (MSA) of the C-terminal tails was performed using the *ggmsa* package, while *seqvisr* was used to visualize gaps and mismatches across the entire alignment. In conjunction, heterogeneity across the sequence was visualized by calculating the degree of difference. This was defined by calculating a conservation score for each residue based on amino acid similarity, scaled from 0 to 1, then taking its complement such that a value of 0 indicated perfect conservation and 1 representing maximal diversity. To visualize overarching patterns in the sequences, values were averaged over bins of 3 residues.

Chicken Eggs and Incubation

Fertilized chicken eggs were obtained from the UC Davis Hopkins Avian Facility at the University of California, Davis and incubated at 37 °C for approximately 3, 4, 5, 6, and 14 days.

Dissection and Fixation

For 3 and 4-day samples, whole embryos were removed and fixed in 2% trichloroacetic acid (TCA) for 30 minutes at room temperature. For 5-day samples, the whole head was removed and fixed in 2% TCA for 40 minutes at room temperature. For 6-day samples, whole eyes were dissected and fixed in 2% TCA for 40 minutes at room temperature. For 14-day samples, only the anterior section of the eye was dissected along the limbal margin. The eyelid and lens were removed before the samples were fixed in 2% TCA for 30 minutes at room temperature.

Immunohistochemistry

Immunohistochemistry (IHC) was performed based on a modified version of the protocol used previously (Echeverria, Leathers et al. 2025), using the primary antibodies listed in Table 3. After dissection and fixation, all samples were washed in 1X PBS (137 mM NaCl, 11.9 mM phosphates, 2.7 mM KCl; pH 7.4) containing

0.1% Triton X-100 (PBST). Samples were incubated in a blocking buffer made up of PBST with 10% donkey serum for 1-7 days at 4 °C. Primary antibodies were diluted in blocking buffer to the indicated dilution and incubated with samples for approximately 72 hours at 4 °C. After primary incubation, samples were washed with PBST then incubated with AlexaFluor secondary antibodies diluted in blocking buffer (1:500) for up to 24 hours at 4 °C. Samples were then washed in PBST and were post-fixed in 4% PFA for 1 hour at room temperature. Tissue samples were also incubated with a DAPI stain (1:500) to mark nuclei. For flat mount imaging (Fig. 6), 6-day dissected corneas subject to IHC were mounted on a slide with Fluoromount-G, coverslipped, and imaged.

After IHC, samples for cross-sectional imaging were prepared for cryosectioning by washing with PBST, then subsequently incubated in 5% sucrose for 12-24 hours at 4 °C, followed by 15% sucrose for 12-24 hours at 4 °C. Samples were then embedded in gelatin and frozen with liquid nitrogen for cryosectioning. Whole mount images were taken of all samples following post-fixation, and transverse sections were taken after cryosectioning using a Thermo Scientific HM525 NX Cryostat.

Fluorescence Imaging and Image Processing

All transverse section images were taken using a Zeiss Axio Imager.M2 with Apotome capability at 10X, 20X, or 63X magnification. Flat mount images (Fig. 6) were taken acquired on a Leica SP8 STED 3X confocal microscope controlled by Leica LAS X software using a 100x/1.4 oil (HC PL APO CS2) object. Z-stacks were acquired with a 0.3-micron step size. All images were deconvolved on-the-fly with Huygens Batch Feeder version 25.10 using the " Standard" strategy (Scientific Volume Imaging, The Netherlands, http://svi.nl). Maximum Intensity Projections (MIP) were generated with Zeiss Zen optical processing software, Imaris (version 10). Imaris and Adobe Photoshop were used for fluorescence image processing. Images shown in manuscript are representative from 3- 9 corneas per marker per stage.

Table 3. Antibodies Used in Study

Antibody Target	Antigen	Dilution	Species Reactivity	Host/Isotype	Source
Tubulin alpha-1A chain (TUBA1A)	Chicken native chick brain microtubules	1:250	human, mouse, gerbil, chicken, rat	Mouse/IgG1	MilliporeSigma
Tubulin alpha-1B chain (TUBA1B)	Recombinant human Tubulin-Alpha protein	1:250	human, mouse, rat, rabbit, monkey, chicken, zebrafish, hamster, goat, p. lividus	Rabbit/IgG	Proteintech
Tubulin alpha-4A chain (TUBA4A)	Full-length protein	1:250	human	Mouse/IgG2b	ThermoFisher
Tubulin beta-2A chain (TUBB2A)	Full-length recombinant protein	1:250	human, mouse, rat	Mouse/IgG2a	Abnova
Tubulin beta-3 chain	Peptide	1:250	human, mouse, rat,	Mouse/IgG1	Proteintech

(TUBB3)			pig, rabbit, chicken		
Neuron-specific beta III Tubulin Antibody	Rat brain-derived microtubules	1:250	Human, Mouse, Rat, Porcine, Amphibian, Avian, Avian, Primate, Transgenic Mouse, Transgenic Rat, Xenograft	Mouse/IgG2a	R&D Systems
N-cadherin (NCAD)	Amino acids 308-597	1:5	Chick, human, mouse, *xenopus*	Rat/IgG2a	DSHB

ACKNOWLEDGEMENTS

The authors acknowledge the members of the Rogers Laboratory at UC Davis School of Veterinary Medicine and the Comparative Ophthalmology and Vision Sciences Laboratory and the for their contributions throughout the study period. Special appreciation to the UC Davis Hopkins Avian Facility for their contiued support.

AUTHOR CONTRIBUTIONS

Conceptualization: R.R, W.R.S., C.D.R., S.M.T.; Data curation: R.R, W.R.S., M.M., S.B..; Formal analysis: R.R, W.R.S.; Funding acquisition: R.R., C.D.R., S.M.T.; Methodology: R.R, W.R.S.; Project administration: R.R., C.D.R., S.M.T.; Resources: C.D.R., S.M.T.; Supervision: R.R, W.R.S., C.D.R., S.M.T.; Visualization: R.R, W.R.S., M.M.; Writing – original draft: R.R, W.R.S. C.D.R.; Writing – review & editing: R.R, W.R.S., C.D.R., S.M.T.

FUNDING

Financial support for this work was provided by grants from: the National Institutes of Health including the National Eye Institute (R01 EY016134 and R01 EY036440) to SMT; National Institute of Dental and Craniofacial Research (NIDCR) R03 DE032047-01, National Science Foundation (NSF) 2143217, and Hypothesis Fund Catalyst Grant to CDR; and the UC Davis Vision Science T32 (NEI-EY015387) to support RR.

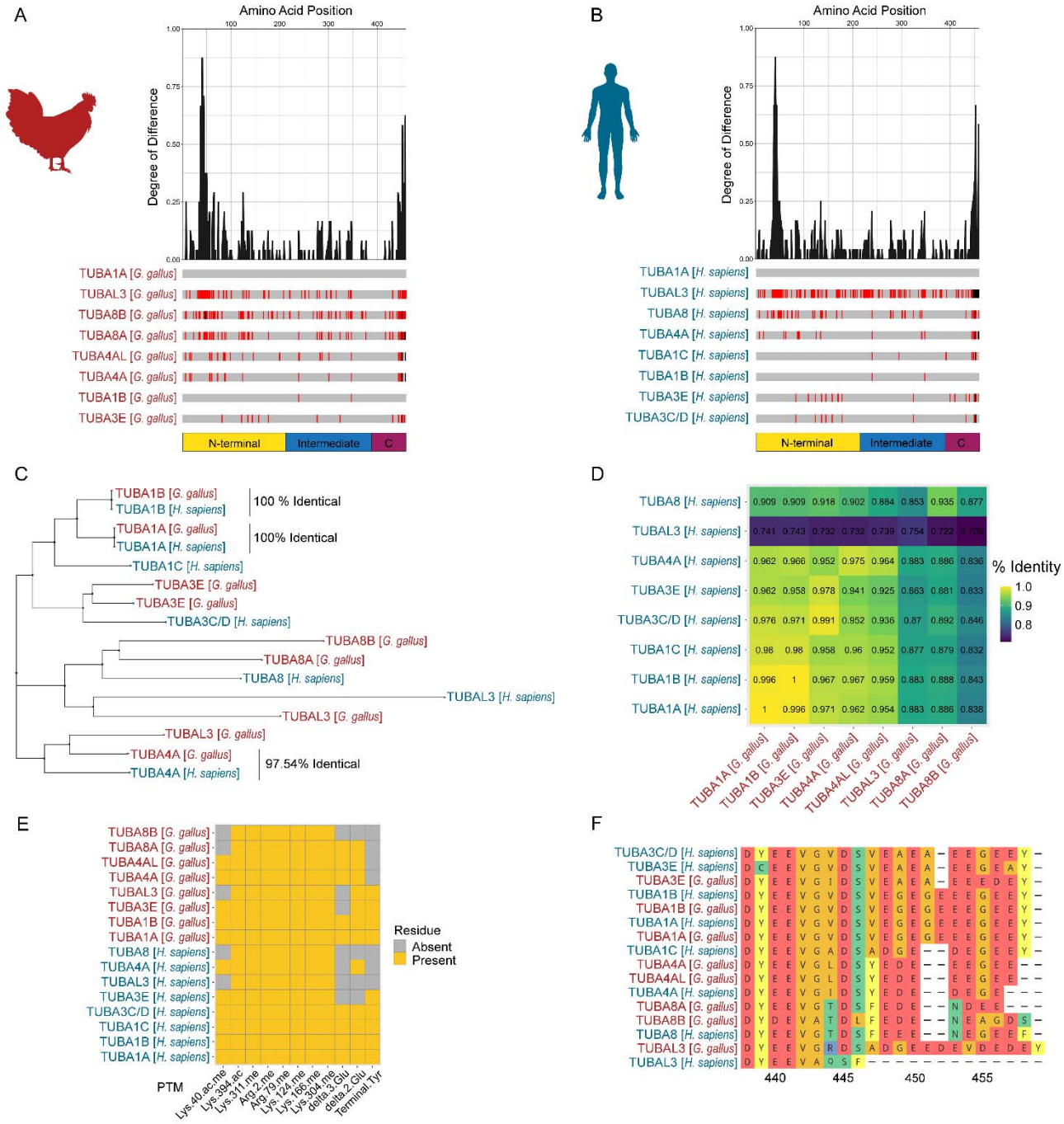

Figure 1. Conservation and divergence of α-tubulin isotypes between chick and human. Chick and human α-tubulin isotypes are highly conserved across core structural domains, with divergence concentrated in C-terminal regions enriched for post-translational modification sites. (A,B) Multiple sequence alignments of α-tubulin isotypes from (A) *Gallus gallus* and (B) *Homo sapiens*. Amino acid mismatches relative to TUBA1A are shown in red, and gaps are shown in black. Plots above each alignment indicate per-residue heterogeneity, calculated as the complement of the conservation score averaged over three-residue bins. (C) Neighbor-joining phylogenetic tree of human and chick α-tubulin isotypes based on amino acid similarity. (D) Pairwise amino acid identity matrix for human and chick α-tubulin isotypes. (E) Distribution of canonical and predicted post-translational modification sites across α-tubulin sequences. Yellow indicates presence of the target residue; grey indicates absence. (F) Alignment of α-tubulin C-terminal tails. Human sequences are shown in blue and chick sequences in red.

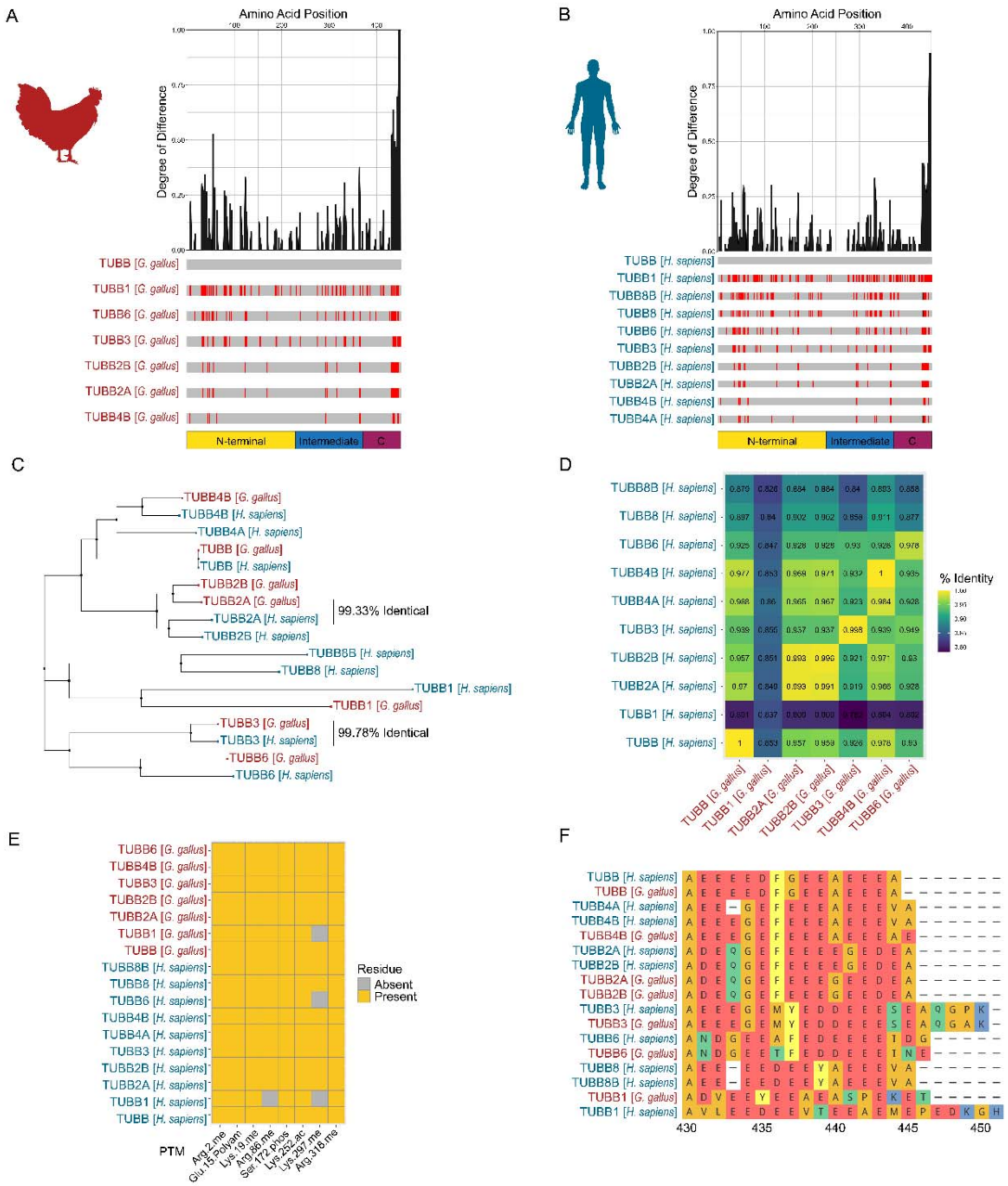

Figure 2. Sequence conservation and divergence of β-tubulin isotypes between chick and human. β-tubulin isotypes show strong cross-species conservation with selective C-terminal divergence, supporting structural conservation alongside potential regulatory specialization. (A,B) Multiple sequence alignments of β-tubulin isotypes from (A) *Gallus gallus* and (B) *Homo sapiens*. Amino acid mismatches relative to TUBA1A are shown in red, and gaps are shown in black. Plots above each alignment indicate per-residue heterogeneity, calculated as the complement of the conservation score averaged over three-residue bins. (C) Neighbor-joining phylogenetic tree of human and chick β-tubulin isotypes based on amino acid similarity. (D) Pairwise amino acid identity matrix for β-tubulin isotypes. (E) Distribution of canonical and predicted post-translational modification sites across β-tubulin sequences. (F) Alignment of β-tubulin C-terminal tails. Human sequences are shown in blue and chick sequences in red.

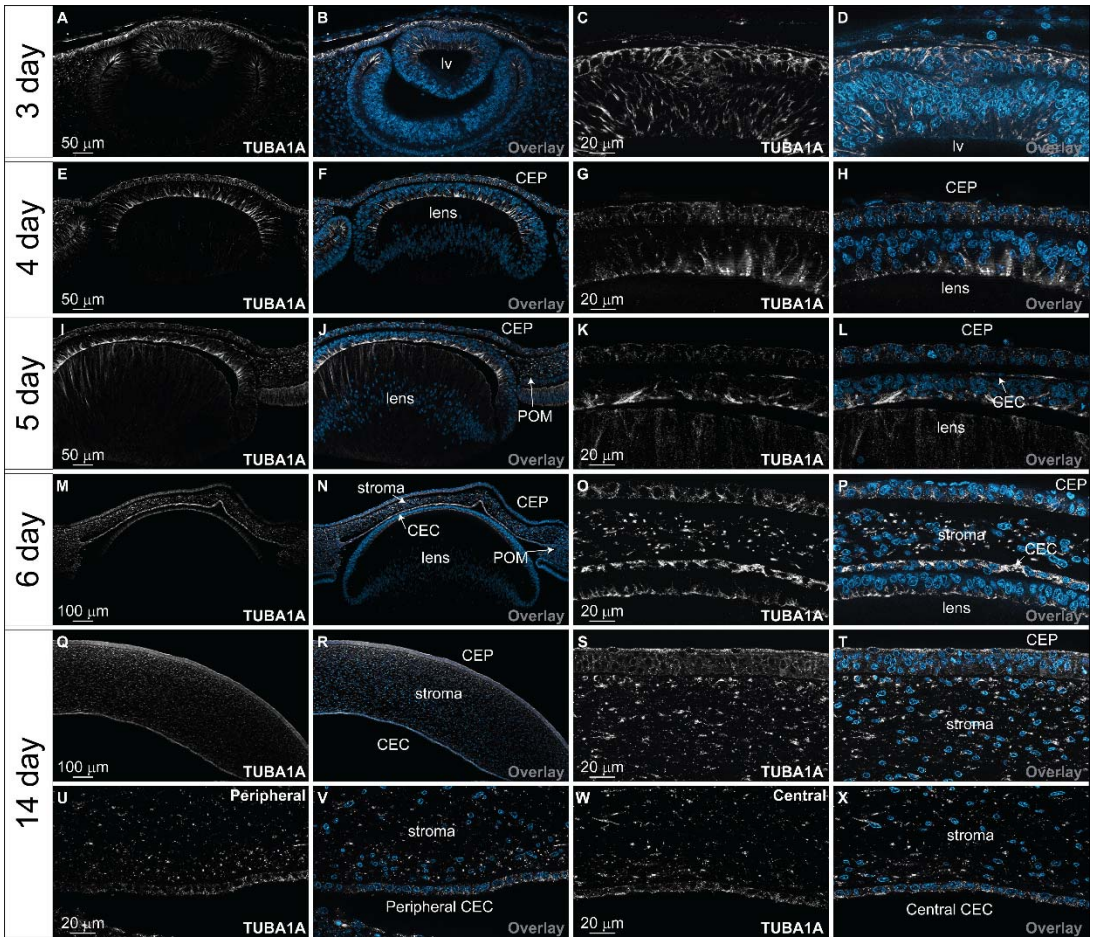

Figure 3. Spatiotemporal localization of TUBA1A during chick corneal development. TUBA1A exhibits broad expression throughout corneal development with stage-dependent redistribution and central enrichment in the mature endothelium. IHC of developing chick eyes at E3, E4, E5, E6, and E14 using antibodies against TUBA1A (white) and DAPI nuclear stain (blue). (A-D) E3 eye showing apical TUBA1A expression in the presumptive corneal epithelium. (E-H) E4 eye showing low, widespread expression during periocular mesenchyme migration. (I-L) E5 eye showing TUBA1A expression in the presumptive corneal endothelium. (M-P) E6 eye showing expression across corneal epithelium, stroma, and endothelium. (Q-X) E14 whole cornea showing strong epithelial and stromal expression. (U-X) Peripheral and central regions of the corneal endothelium at E14, showing central enrichment of TUBA1A. All sections are anterior to the top and posterior to the bottom. N= 3 corneas assessed for all stages.

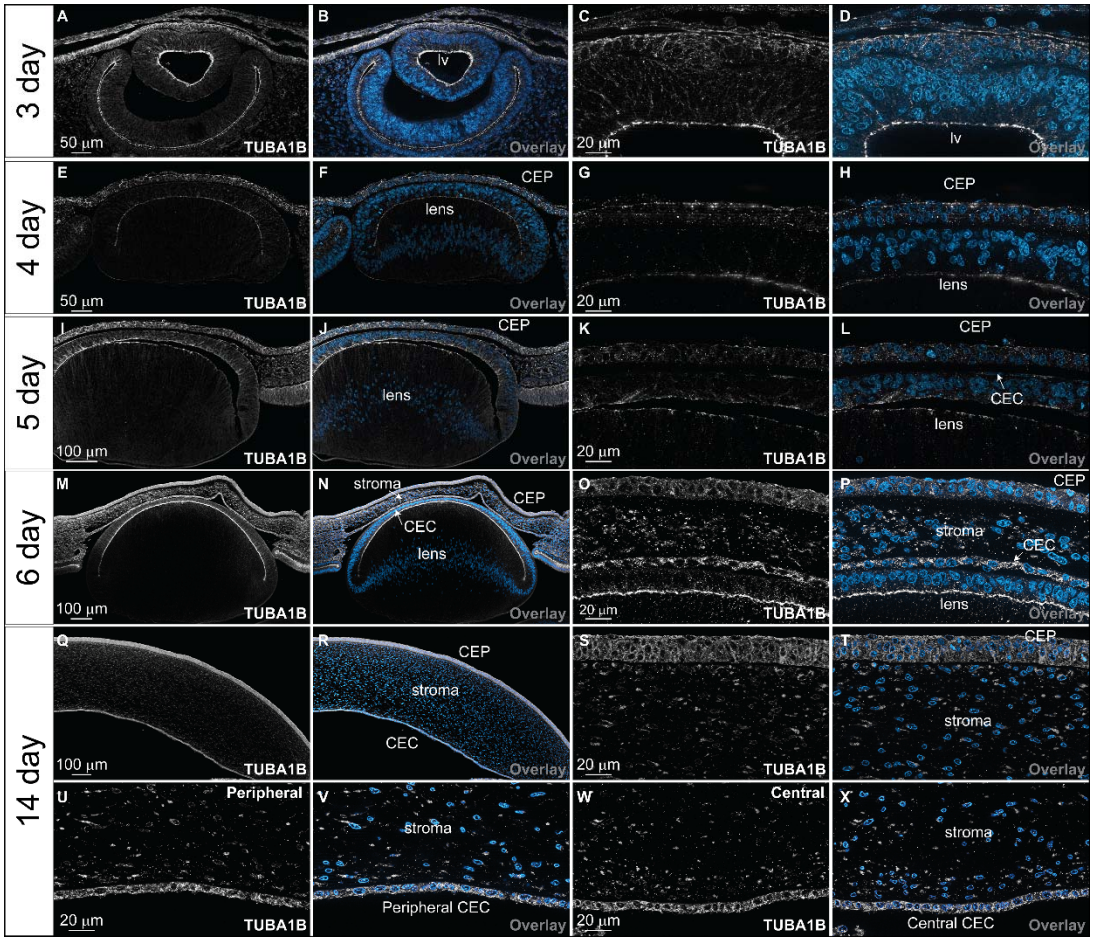

Figure 4. Spatiotemporal localization of TUBA1B during chick corneal development. TUBA1B is broadly and consistently expressed across corneal layers, displaying sustained epithelial enrichment and relatively uniform endothelial distribution. IHC of developing chick eyes at E3, E4, E5, E6, and E14 using antibodies against TUBA1B (white) and DAPI nuclear stain (blue). (A-A□) E3 eye showing low-level, widespread expression in the surface ectoderm with apical enrichment in the presumptive corneal epithelium. (B-B□) E4 eye showing continued epithelial expression during periocular mesenchyme migration. (C-C□) E5 eye showing expression in the presumptive corneal endothelium. (D-D□) E6 eye showing cytoplasmic expression across corneal epithelium, stroma, and endothelium. (E-E□) E14 whole cornea showing robust expression in stratifying epithelium and stroma. (F-F□) Central and peripheral regions of the corneal endothelium at E14 showing uniform endothelial expression. All sections are anterior to the top and posterior to the bottom. N= 3 (3 day), 5 (4 day), 4 (5 day), 5 (6 day) and 3 (14 day) corneas assessed for all stages.

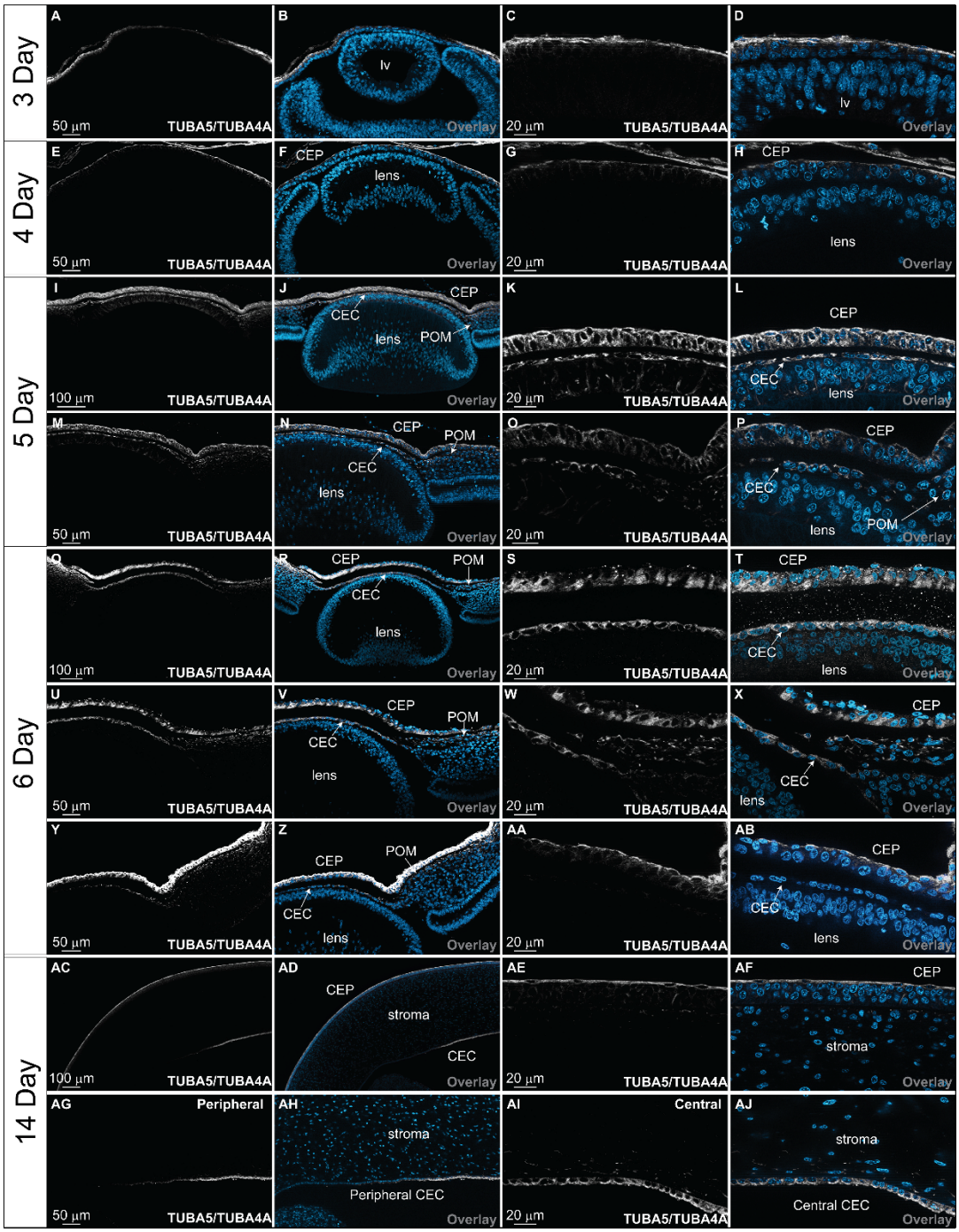

Figure 5. Dynamic and spatially restricted localization of TUBA5/TUBA4A during corneal development. TUBA5/TUBA4A shows dynamic, spatially restricted redistribution during corneal morphogenesis, with stage-specific shifts and central enrichment in the mature endothelium. IHC of developing chick eyes at E3, E4, E5, E6, and E14 using antibodies against TUBA5/TUBA4A (white) and DAPI nuclear stain (blue). (A-D) E3 eye showing apical expression in the presumptive corneal epithelium. (E-H) E4 eye showing increased apical epithelial expression. (I-P) E5 eye showing expression in the corneal epithelium, presumptive corneal endothelium, and anterior periocular mesenchyme. (O-AB) E6 eye showing basal localization in epithelium and endothelium and expression in migrating stromal precursors. (AC-AJ) E14 whole cornea showing expression restricted to epithelium and endothelium. (AG-AJ) Central and peripheral regions of the corneal endothelium at E14 showing central enrichment and apical bias. All sections are anterior to the top and posterior to the bottom. N= 3 (3 day), 3 (4 day), 4 (5 day), 4 (6 day) and 3 (14 day) corneas assessed for all stages.

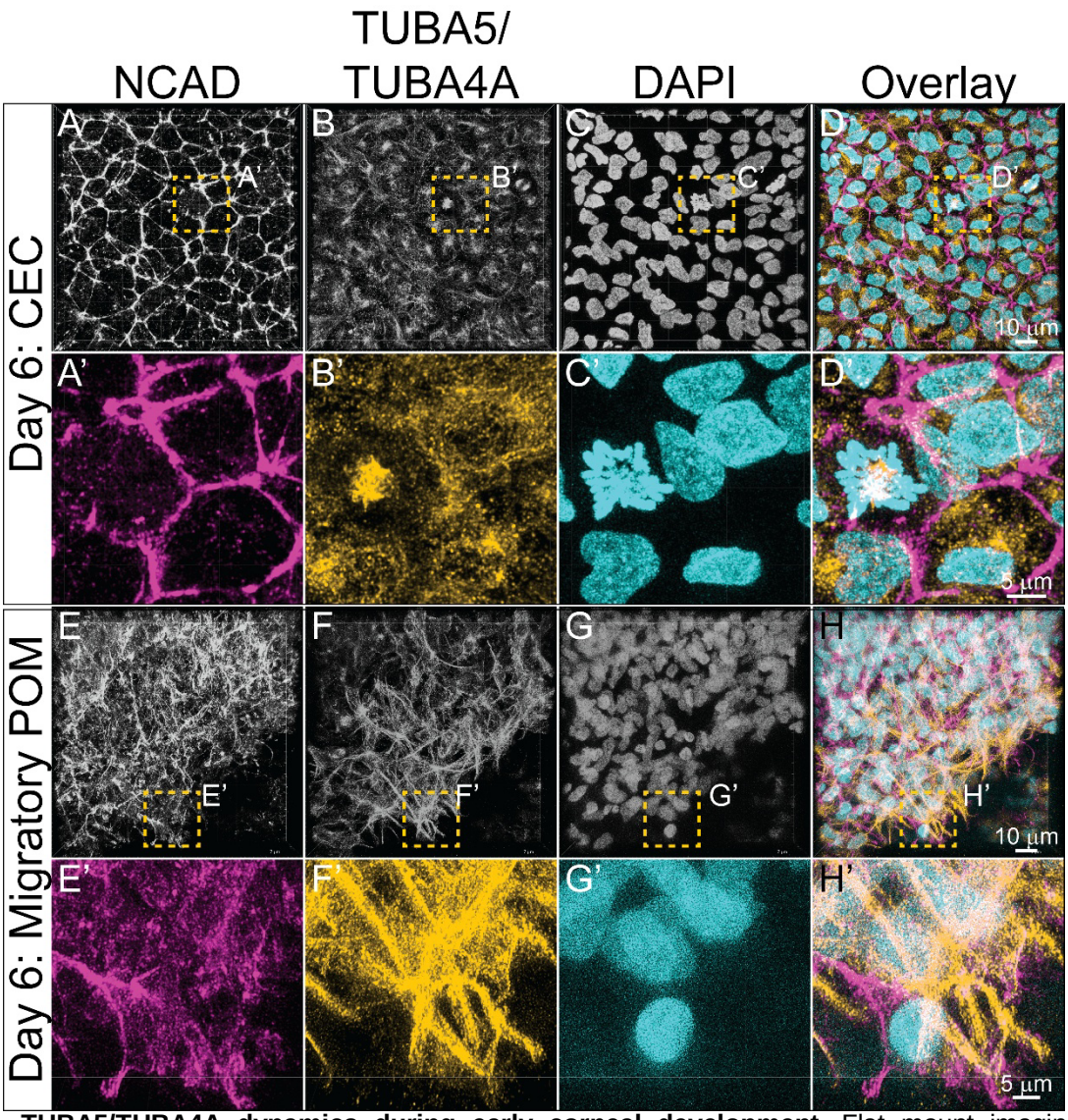

Figure 6. TUBA5/TUBA4A dynamics during early corneal development. Flat mount imaging reveals context-dependent TUBA5/TUBA4A organization, with diffuse peri-membranous distribution in endothelial cells and prominent bundled microtubules in migratory mesenchyme. IHC of corneal flat mounts at E6 using antibodies against NCAD (magenta), TUBA5/TUBA4A (yellow) and DAPI (cyan). (A-D) E6 corneal endothelial maximum intensity projections (MIP) show discrete NCAD boundaries with diffusive distribution of small diameter TUBA5/TUBA4A microtubules. (A'-D') Subsection of MIP shows membrane NCAD marking, diffuse peri-membranous and centrosomal TUBA4A staining in corneal endothelia. (E-H) E6 migratory periocular mesenchyme MIP show diffuse NCAD staining with discrete large diameter TUBA5/TUBA4A microtubules biased towards the leading edge. (E'-H') Subsection of MIP highlights predominantly diffuse and minor punctate NCAD staining in addition to large TUBA5/TUBA4A microtubules. N= 9 corneas assessed for 6-day flat mounts.

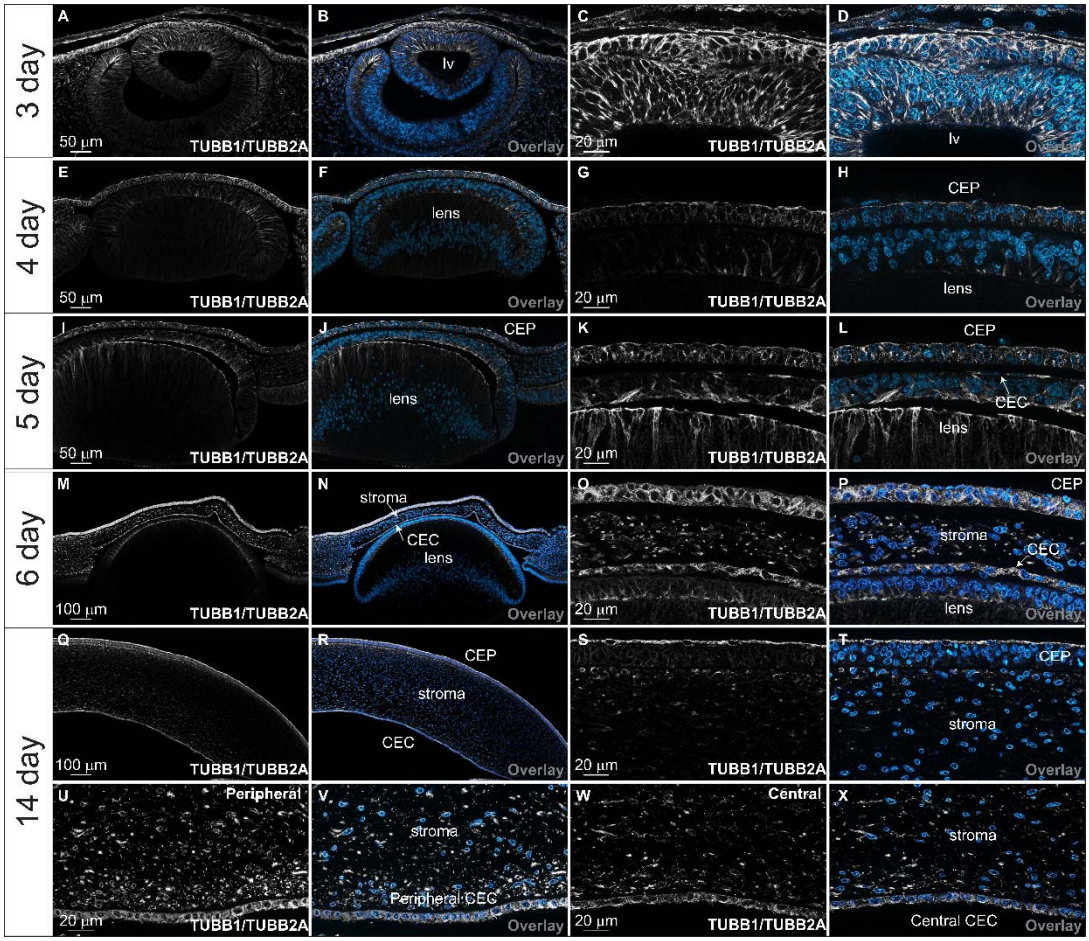

Figure 7. Developmental redistribution of TUBB1/TUBB2A in corneal tissues. TUBB1/TUBB2A undergoes developmental redistribution across corneal tissues, transitioning from broad early epithelial expression to polarized enrichment in mature layers. IHC of developing eye after 3, 4, 5, 6 and 14 days of incubation with antibodies against TUBB1/TUBB2A protein (white) and DAPI. (A-D) E3 eye showing broad epithelial expression with apical enrichment. (E-H) E4 eye showing continued epithelial and periocular mesenchyme expression. (I-L) E5 eye showing reduced epithelial apical signal and increased endothelial expression. (M-P) E6 eye showing cytoplasmic expression across corneal layers. (Q-T) E14 whole cornea showing apical epithelial expression and stromal localization. (U-X) Central and peripheral regions of the corneal endothelium at E14 showing central enrichment and apical bias. All sections are anterior to the top and posterior to the bottom. N= 3 corneas assessed for all stages.

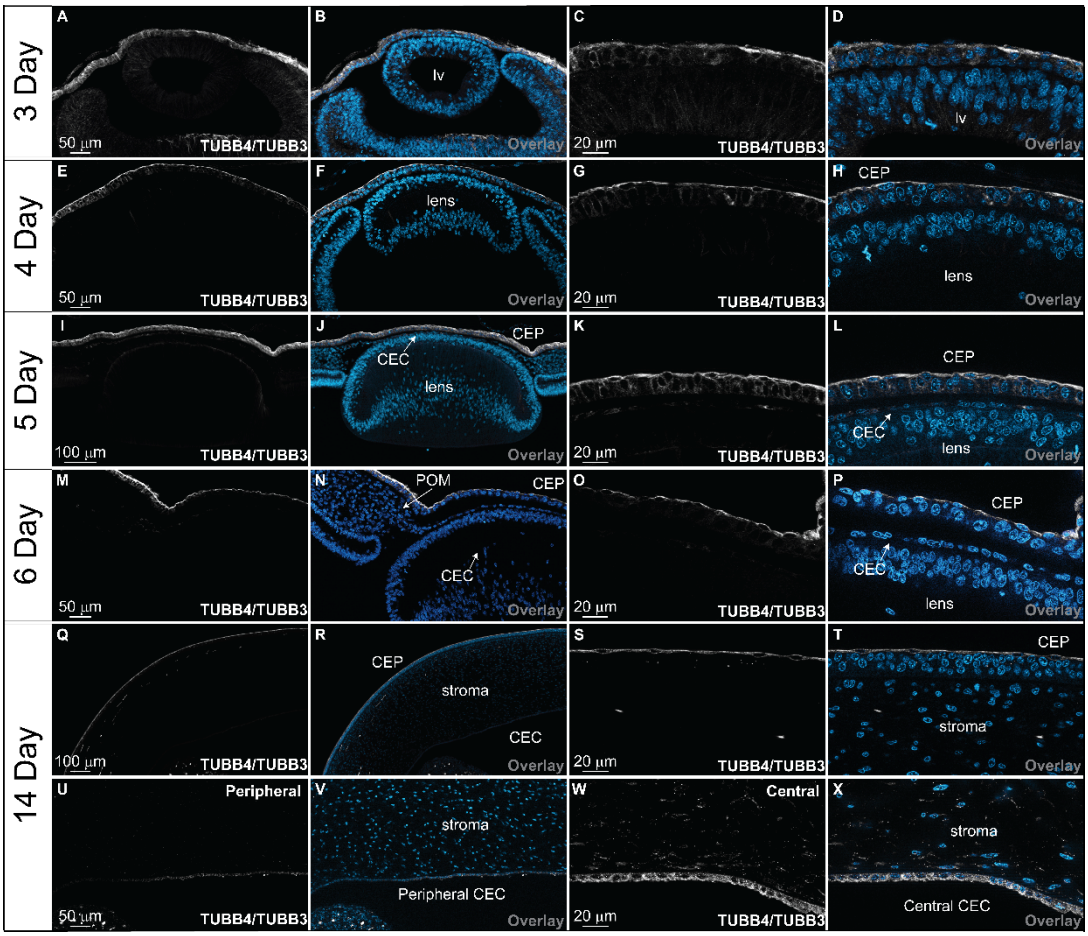

Figure 8. Polarized expression of TUBB4/TUBB3 in corneal epithelium, endothelium, and stromal nerves. TUBB4/TUBB3 displays polarized apical epithelial localization throughout development and selectively labels stromal nerves in the mature cornea. IHC of developing chick eyes at E3, E4, E5, E6, and E14 using antibodies against TUBB4/TUBB3 (white) and DAPI nuclear stain (blue). (A-A□) E3 eye showing apical epithelial expression. (B-B□) E4 eye showing sustained apical localization. (C-C□) E5 eye showing apical epithelial expression and limited endothelial signal. (D-D□) E6 eye showing similar epithelial localization with low endothelial expression. (E-E□) E14 whole cornea showing strong apical epithelial expression and stromal nerve labeling. (F-F□) Central and peripheral regions of the corneal endothelium at E14 showing central enrichment and apical bias. All sections are anterior to the top and posterior to the bottom. N= 3 (3 day), 4 (4 day), 3 (5 day), 4 (6 day) and 3 (14 day) corneas assessed for all stages.

REFERENCES

Aiken, J., G. Buscaglia, E. A. Bates and J. K. Moore (2017). "The alpha-Tubulin gene TUBA1A in Brain Development: A Key Ingredient in the Neuronal Isotype Blend." J Dev Biol **5**(3).

Bao, M., R. E. Dorig, P. M. Vazquez-Pianzola, D. Beuchle and B. Suter (2023). "Differential modification of the C-terminal tails of different alpha-tubulins and their importance for microtubule function in vivo." Elife **12**.

Bar, J., Y. Popp, M. Bucher and M. Mikhaylova (2022). "Direct and indirect effects of tubulin post-translational modifications on microtubule stability: Insights and regulations." Biochim Biophys Acta Mol Cell Res **1869**(6): 119241.

Benkirane, M., M. Bonhomme, H. Morsy, S. L. Safgren, C. Marelli, A. Chaussenot, D. Smedley, V. Cipriani, J. M. de Sainte-Agathe, C. Ding, L. Larrieu, L. Vestito, H. Margot, G. Lesca, F. Ramond, A. Castrioto, D. Baux, J. Verheijen, E. Sansa, P. Giunti, A. Haetty, A. Bergougnoux, M. Pointaux, O. Ardouin, C. Van Goethem, M. C. Vincent, M. Hadjivassiliou, M. Cossee, T. Rouaud, O. Bartsch, W. D. Freeman, K. J. Wierenga, E. W. Klee, J. Vandrovcova, H. Houlden, A. Debant and M. Koenig (2024). "De novo and inherited monoallelic variants in TUBA4A cause ataxia and spasticity." Brain **147**(11): 3681-3689.

Bonanno, J. A. (2012). "Molecular mechanisms underlying the corneal endothelial pump." Exp Eye Res **95**(1): 2-7.

Carmona, B., H. S. Marinho, C. L. Matos, S. Nolasco and H. Soares (2023). "Tubulin Post-Translational Modifications: The Elusive Roles of Acetylation." Biology (Basel) **12**(4).

Chacon, J. and C. D. Rogers (2019). "Early expression of Tubulin Beta-III in avian cranial neural crest cells." Gene Expr Patterns **34**: 119067.

Chen, Y. F. and C. Y. Dong (2022). "Dynamic development of the extracellular matrix in chick cornea." J Biophotonics **15**(3): e202100210.

Chew, S., R. Balasubramanian, W. M. Chan, P. B. Kang, C. Andrews, B. D. Webb, S. E. MacKinnon, D. T. Oystreck, J. Rankin, T. O. Crawford, M. Geraghty, S. L. Pomeroy, W. F. Crowley, Jr., E. W. Jabs, D. G. Hunter, P. E. Grant and E. C. Engle (2013). "A novel syndrome caused by the E410K amino acid substitution in the neuronal beta-tubulin isotype 3." Brain **136**(Pt 2): 522-535.

Downing, K. H. and E. Nogales (1998). "Tubulin structure: insights into microtubule properties and functions." Curr Opin Struct Biol **8**(6): 785-791.

Echeverria, C. V., Jr., T. A. Leathers and C. D. Rogers (2025). "Comparative analysis of fixation techniques for signal detection in avian embryos." Dev Biol **517**: 13-23.

Eghrari, A. O., S. A. Riazuddin and J. D. Gottsch (2015). "Overview of the Cornea: Structure, Function, and Development." Prog Mol Biol Transl Sci **134**: 7-23.

Etienne-Manneville, S. (2013). "Microtubules in cell migration." Annu Rev Cell Dev Biol **29**: 471-499.

Fernandes, V. M., K. McCormack, L. Lewellyn and E. M. Verheyen (2014). "Integrins regulate apical constriction via microtubule stabilization in the Drosophila eye disc epithelium." Cell Rep **9**(6): 2043-2055.

Gadadhar, S., S. Bodakuntla, K. Natarajan and C. Janke (2017). "The tubulin code at a glance." J Cell Sci **130**(8): 1347-1353.

Ganne, A., M. Balasubramaniam, H. Ayyadevara, L. Kiaei, R. J. Shmookler Reis, K. I. Varughese and M. Kiaei (2023). "In silico analysis of TUBA4A mutations in Amyotrophic Lateral Sclerosis to define mechanisms of microtubule disintegration." Sci Rep **13**(1): 2096.

Garcin, C. and A. Straube (2019). "Microtubules in cell migration." Essays Biochem **63**(5): 509-520.

Hao, X. D., P. Chen, Y. Y. Zhang, S. X. Li, W. Y. Shi and H. Gao (2017). "De novo mutations of TUBA3D are associated with keratoconus." Sci Rep **7**(1): 13570.

Hausrat, T. J., J. Radwitz, F. L. Lombino, P. Breiden and M. Kneussel (2021). "Alpha- and beta-tubulin isotypes are differentially expressed during brain development." Dev Neurobiol **81**(3): 333-350.

Janke, C. (2014). "The tubulin code: molecular components, readout mechanisms, and functions." J Cell Biol **206**(4): 461-472.

Janke, C. and M. M. Magiera (2020). "The tubulin code and its role in controlling microtubule properties and functions." Nat Rev Mol Cell Biol **21**(6): 307-326.

Joseph, R., O. P. Srivastava and R. R. Pfister (2011). "Differential epithelial and stromal protein profiles in keratoconus and normal human corneas." Exp Eye Res **92**(4): 282-298.

Jouhilahti, E. M., S. Peltonen and J. Peltonen (2008). "Class III beta-tubulin is a component of the mitotic spindle in multiple cell types." J Histochem Cytochem **56**(12): 1113-1119.
Kalutskii, M., H. Grubmuller, V. A. Volkov and M. Igaev (2025). "Microtubule dynamics are defined by conformations and stability of clustered protofilaments." Proc Natl Acad Sci U S A **122**(22): e2424263122.
Katsetos, C. D., M. M. Herman and S. J. Mork (2003). "Class III beta-tubulin in human development and cancer." Cell Motil Cytoskeleton **55**(2): 77-96.
Kivela, T. and M. Uusitalo (1998). "Structure, development and function of cytoskeletal elements in non-neuronal cells of the human eye." Prog Retin Eye Res **17**(3): 385-428.
Kristensson, M. A. (2021). "The Game of Tubulins." Cells **10**(4).
Laan, L., J. Husson, E. L. Munteanu, J. W. Kerssemakers and M. Dogterom (2008). "Force-generation and dynamic instability of microtubule bundles." Proc Natl Acad Sci U S A **105**(26): 8920-8925.
Linge, A., S. Kennedy, D. O'Flynn, S. Beatty, P. Moriarty, M. Henry, M. Clynes, A. Larkin and P. Meleady (2012). "Differential expression of fourteen proteins between uveal melanoma from patients who subsequently developed distant metastases versus those who did Not." Invest Ophthalmol Vis Sci **53**(8): 4634-4643.
Liu, G. Y., S. C. Chen, G. H. Lee, K. Shaiv, P. Y. Chen, H. Cheng, S. R. Hong, W. T. Yang, S. H. Huang, Y. C. Chang, H. C. Wang, C. L. Kao, P. C. Sun, M. H. Chao, Y. Y. Lee, M. J. Tang and Y. C. Lin (2022). "Precise control of microtubule disassembly in living cells." EMBO J **41**(15): e110472.
Lwigale, P. Y. (2015). "Corneal Development: Different Cells from a Common Progenitor." Prog Mol Biol Transl Sci **134**: 43-59.
Magiera, M. M. (2023). "The tubulin code: Empowering microtubules." Semin Cell Dev Biol **137**: 1-2.
Moutin, M. J., C. Bosc, L. Peris and A. Andrieux (2021). "Tubulin post-translational modifications control neuronal development and functions." Dev Neurobiol **81**(3): 253-272.
Myers, K. A., L. E. Bello-Espinosa, A. Kherani, X. C. Wei and A. M. Innes (2015). "TUBA1A Mutation Associated With Eye Abnormalities in Addition to Brain Malformation." Pediatr Neurol **53**(5): 442-444.
Nakagawa, T., N. Okumura, M. Ikegawa, Y. Toyama, T. Nirasawa, F. Mascarelli, H. Vaitinadapoule, I. Aouimeur, Z. He, P. Gain, G. Thuret and N. Koizumi (2023). "Shotgun proteomics identification of proteins expressed in the Descemet's membrane of patients with Fuchs endothelial corneal dystrophy." Sci Rep **13**(1): 10401.
Ong Tone, S., V. Kocaba, M. Bohm, A. Wylegala, T. L. White and U. V. Jurkunas (2021). "Fuchs endothelial corneal dystrophy: The vicious cycle of Fuchs pathogenesis." Prog Retin Eye Res **80**: 100863.
Paturle-Lafanechere, L., M. Manier, N. Trigault, F. Pirollet, H. Mazarguil and D. Job (1994). "Accumulation of delta 2-tubulin, a major tubulin variant that cannot be tyrosinated, in neuronal tissues and in stable microtubule assemblies." J Cell Sci **107 (Pt 6)**: 1529-1543.
Plochocka, A. Z., M. Ramirez Moreno, A. M. Davie, N. A. Bulgakova and L. Chumakova (2021). "Robustness of the microtubule network self-organization in epithelia." Elife **10**.
Ritchey, E. R., K. Code, C. P. Zelinka, M. A. Scott and A. J. Fischer (2011). "The chicken cornea as a model of wound healing and neuronal re-innervation." Mol Vis **17**: 2440-2454.
Sanyal, C., N. Pietsch, S. Ramirez Rios, L. Peris, L. Carrier and M. J. Moutin (2023). "The detyrosination/re-tyrosination cycle of tubulin and its role and dysfunction in neurons and cardiomyocytes." Semin Cell Dev Biol **137**: 46-62.
Schroter, J., J. H. Doring, S. F. Garbade, G. F. Hoffmann, S. Kolker, M. Ries and S. Syrbe (2021). "Cross-sectional quantitative analysis of the natural history of TUBA1A and TUBB2B tubulinopathies." Genet Med **23**(3): 516-523.
Schroter, J., B. Popp, H. Brennenstuhl, J. H. Doring, S. H. Donze, E. K. Bijlsma, A. van Haeringen, D. Huhle, L. Jestaedt, A. Merkenschlager, M. Arelin, D. Grafe, S. Neuser, S. Oates, D. K. Pal, M. J. Parker, J. R. Lemke, G. F. Hoffmann, S. Kolker, I. Harting and S. Syrbe (2022). "Complementing the phenotypical spectrum of TUBA1A tubulinopathy and its role in early-onset epilepsies." Eur J Hum Genet **30**(3): 298-306.
Su, C. C., V. Desikan, K. Betsch, M. S. Shim, K. E. Keller and P. B. Liton (2025). "Tubulin Acetylation Enhances Microtubule Stability in Trabecular Meshwork Cells Under Mechanical Stress." Invest Ophthalmol Vis Sci **66**(1): 43.
Takeda, M., M. M. Sami and Y. C. Wang (2018). "A homeostatic apical microtubule network shortens cells for epithelial folding via a basal polarity shift." Nat Cell Biol **20**(1): 36-45.
Tischfield, M. A., H. N. Baris, C. Wu, G. Rudolph, L. Van Maldergem, W. He, W. M. Chan, C. Andrews, J. L. Demer, R. L. Robertson, D. A. Mackey, J. B. Ruddle, T. D. Bird, I. Gottlob, C. Pieh, E. I. Traboulsi, S. L.

Pomeroy, D. G. Hunter, J. S. Soul, A. Newlin, L. J. Sabol, E. J. Doherty, C. E. de Uzcategui, N. de Uzcategui, M. L. Collins, E. C. Sener, B. Wabbels, H. Hellebrand, T. Meitinger, T. de Berardinis, A. Magli, C. Schiavi, M. Pastore-Trossello, F. Koc, A. M. Wong, A. V. Levin, M. T. Geraghty, M. Descartes, M. Flaherty, R. V. Jamieson, H. U. Moller, I. Meuthen, D. F. Callen, J. Kerwin, S. Lindsay, A. Meindl, M. L. Gupta, Jr., D. Pellman and E. C. Engle (2010). "Human TUBB3 mutations perturb microtubule dynamics, kinesin interactions, and axon guidance." Cell **140**(1): 74-87.

Tischfield, M. A., G. Y. Cederquist, M. L. Gupta, Jr. and E. C. Engle (2011). "Phenotypic spectrum of the tubulin-related disorders and functional implications of disease-causing mutations." Curr Opin Genet Dev **21**(3): 286-294.

Torella, A., I. Ricca, G. Piluso, D. Galatolo, G. De Michele, M. Zanobio, R. Trovato, G. De Michele, R. Zeuli, C. Pane, S. Cocozza, F. Sacca, F. M. Santorelli, V. Nigro and A. Filla (2023). "A new genetic cause of spastic ataxia: the p.Glu415Lys variant in TUBA4A." J Neurol **270**(10): 5057-5063.

Verhey, K. J. and J. Gaertig (2007). "The tubulin code." Cell Cycle **6**(17): 2152-2160.

Wan, Y., C. Zhou, X. Chang, L. Wu, Y. Zheng, J. Yu, L. Bai, M. Luan, M. Yu, Q. Wang, W. Zhang, Y. Yuan, J. Deng and Z. Wang (2024). "Novel TUBA4A variant causes congenital myopathy with focal myofibrillar disorganisation." J Med Genet **61**(7): 626-632.

Weinreb, R. N. and M. I. Ryder (1990). "In situ localization of cytoskeletal elements in the human trabecular meshwork and cornea." Invest Ophthalmol Vis Sci **31**(9): 1839-1847.

Wen, Y., C. Ren, L. Zhu, L. Huang, H. Qi, W. Yu, K. Wang, M. Zhao and Q. Xu (2024). "Unmasking of molecular players: proteomic profiling of vitreous humor in pathologic myopia." BMC Ophthalmol **24**(1): 352.

Wethekam, L. C. and J. K. Moore (2022). "Microtubule cytoskeleton: Revealing new readers of the tubulin code." Curr Biol **32**(18): R960-R962.

Whitman, M. C., C. Andrews, W. M. Chan, M. A. Tischfield, S. F. Stasheff, F. Brancati, X. Ortiz-Gonzalez, S. Nuovo, F. Garaci, S. E. MacKinnon, D. G. Hunter, P. E. Grant and E. C. Engle (2016). "Two unique TUBB3 mutations cause both CFEOM3 and malformations of cortical development." Am J Med Genet A **170A**(2): 297-305.

Yan, J., S. Mehta, K. Patel, N. Dhupar, N. Little and S. Ong Tone (2024). "Transcription factor 4 promotes increased corneal endothelial cellular migration by altering microtubules in Fuchs endothelial corneal dystrophy." Sci Rep **14**(1): 10276.

Yeniay Sut, N., M. Yildirim, O. Bektas, M. Altintas and S. Teber (2022). "The diagnostic challenges of congenital mirror movements and hand stereotypies in a case with TUBB3-associated tubulinopathy." Acta Neurol Belg **122**(1): 251-253.

Yon, W. J., T. Ha, Y. Zheng and R. T. A. Pedersen (2025). "A tubulin-binding protein that preferentially binds to GDP-tubulin and promotes GTP exchange." J Biol Chem **301**(8): 110401.